Nucleic Acids Research, 2023, **51**, 11277–11290
https://doi.org/10.1093/nar/gkad794
Advance access publication date: 9 October 2023
RNA and RNA-protein complexes

Yeast ribosome biogenesis factors Puf6 and Nog2 and ribosomal proteins uL2 and eL43 act in concert to facilitate the release of nascent large ribosomal subunits from the nucleolus

Amber J. LaPeruta, Stefanie Hedayati, Jelena Micic, Fiona Fitzgerald, David Kim, Grace Oualline and John L. Woolford*

Department of Biological Sciences, Carnegie Mellon University, Pittsburgh, PA 15213, USA
*To whom correspondence should be addressed. Tel: +1 412 268 3193; Fax: +1 412 268 7129; Email: jw17@andrew.cmu.edu

Abstract

Large ribosomal subunit precursors (pre-LSUs) are primarily synthesized in the nucleolus. At an undetermined step in their assembly, they are released into the nucleoplasm. Structural models of yeast pre-LSUs at various stages of assembly have been collected using cryo-EM. However, which cryo-EM model is closest to the final nucleolar intermediate of the LSU has yet to be determined. To elucidate the mechanisms of the release of pre-LSUs from the nucleolus, we assayed effects of depleting or knocking out two yeast ribosome biogenesis factors (RiBi factors), Puf6 and Nog2, and two ribosomal proteins, uL2 and eL43. These proteins function during or stabilize onto pre-LSUs between the late nucleolar stages to early nucleoplasmic stages of ribosome biogenesis. By characterizing the phenotype of these four mutants, we determined that a particle that is intermediate between the cryo-EM model State NE1 and State NE2 likely represents the final nucleolar assembly intermediate of the LSU. We conclude that the release of the RiBi factors Nip7, Nop2 and Spb1 and the subsequent stabilization of rRNA domains IV and V may be key triggers for the release of pre-LSUs from the nucleolus.

Graphical abstract

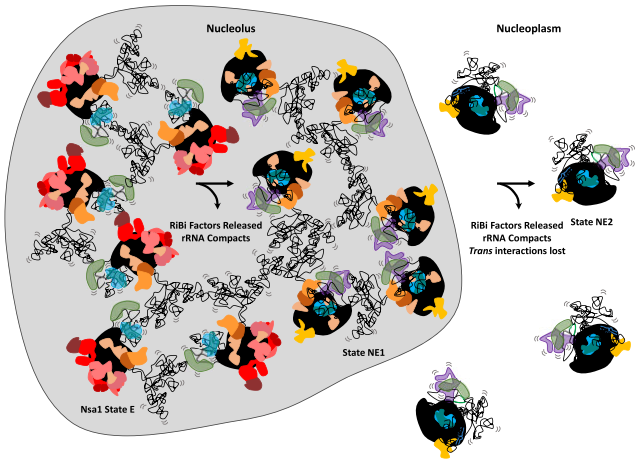

Introduction

Ribosome biogenesis is a multistep process that spans three cellular compartments: it is initiated in the nucleolus, continues in the nucleoplasm, and concludes in the cytoplasm. This process has been best studied in the yeast *Saccharomyces cerevisiae*. In the nucleolus, transcription of the 35S precursor rRNA (pre-rRNA) marks the beginning of the ribosome assembly pathway. This transcript contains sequences for the 18S rRNA of the mature small ribosomal subunit (SSU) and the 5.8S and 25S rRNAs of the large ribosomal subunit (LSU),flanked and separated by transcribed spacer sequences (Supplementary Figure S1) (1–3). The 5S rRNA of the LSU is transcribed separately. Folding, compaction, modification, and processing of pre-rRNA, and stable integration of ribosomal proteins (RPs) occurs primarily in the nucleolus. Pre-ribosomes undergo final stages of maturation following

Received: April 15, 2022. **Revised:** September 11, 2023. **Editorial Decision:** September 18, 2023. **Accepted:** September 22, 2023

exit from the nucleolus into the nucleoplasm and then export to the cytoplasm. More than 200 ribosome biogenesis factors (RiBi factors) associate with and are released from pre-ribosomes at different times to facilitate accurate and efficient ribosome assembly (1–3). Assays of RiBi factor mutants and examination of cryo-EM structures of yeast ribosome assembly intermediates suggest that these RiBi factors enable significant remodeling of RNA-RNA, RNA-protein, and protein-protein interactions required to drive assembly forward (4). However, a detailed understanding of the dynamics of ribosome assembly remains to be elucidated.

The nucleolus is a biomolecular condensate formed by liquid-liquid phase separation, which is thought to be mediated by multiple transient, weak interactions between pre-ribosomes and other nucleolar components (4–6). Consequently, the morphology of the nucleolus is dependent on, and interconnected with, ribosome biogenesis (7–9). For example, defects in ribosome biogenesis in humans (ribosomopathies) are often associated with cancers and other diseases that exhibit abnormal shape or size of the nucleolus (9,10).

While ribosome assembly contributes to the formation and maintenance of the nucleolus, it remains unclear how this occurs, and when and how nascent ribosomes are released from the nucleolar condensate. It seems likely that a decrease in the number of *trans* interactions between pre-ribosomes and other components of the nucleolus enables their release from the nucleolus (4,6). What little is known about the release of pre-ribosomes from the nucleolus *in vivo* has been learned through studies of ribosome assembly in *S. cerevisiae*. Cryo-EM structures have captured snapshots of precursor LSUs (pre-LSUs) as they assemble in the nucleolus and the nucleoplasm. Examination of these structures, and how their composition changes as they mature, provide hints for how pre-ribosomes are released from the nucleolus into the nucleoplasm (4). However, we do not yet know exactly which, if any, of the available cryo-EM structures represents the last nucleolar intermediate. Four stable cryo-EM structures, or intermediates between these structures that are yet to be discovered, are candidates for being the final nucleolar intermediate: Nsa1 State E, State NE1, State NE2 and Nog2 State 1 (Figure 1). The Nsa1 State E cryo-EM model is believed to be a nucleolar intermediate because it was isolated from the *ytm1E80A* mutant in which the release of pre-LSUs from the nucleolus is blocked (11,12). In this mutant, ytm1E80A and several other RiBi factors are not released from pre-LSUs, preventing extensive remodeling of the nascent particles (11,12). Nog2 State 1 is thought to be the earliest nucleoplasmic ribosome assembly intermediate because the pre-LSUs analyzed to form this model were purified using the RiBi factor Nog2, which primarily localizes to the nucleoplasm (12–14). However, because Nog2-eGFP also partially localizes to the nucleolus, some pre-LSUs purified using Nog2 as bait might be nucleolar. Thus, Nog2 State 1 is another candidate for the last nucleolar intermediate. Finally, one of the two intermediate structures present during the transition from Nsa1 State E to Nog2 State 1, namely State NE1 and State NE2, could also represent the final nucleolar assembly intermediate of the nascent LSU. These two structures were created based on pre-LSUs that were isolated using the RiBi factor Nop53 as bait (15). Nop53 associates with pre-LSUs in the nucleolus and is released when the internal transcribed spacer sequence ITS2 is processed in the nucleoplasm (16).

During the transition between Nsa1 State E and State NE1, seven strictly nucleolar RiBi factors are released from pre-LSUs. Additionally, the RPs uL2 and eL43 and a small portion of Nog2 are first visualized by cryo-EM (Figure 1A) (12,15,17). Three RiBi factors that remain bound to the pre-LSU, Nip7, Nop2 and Spb1, likely prevent the compaction of the last two of the six rRNA domains of the large ribosomal subunit, rRNA domains IV and V, onto the pre-LSU in the State NE1 structure (Figure 1A). This is because the position of these proteins on the structure should sterically hinder movement of rRNA helices toward their mature conformation. Thus, we refer to Nip7, Nop2 and Spb1 as 'rRNA steric hindrance factors'. Given that *trans* interactions between RNA and other components of the nucleolus are thought to play a significant role in the retention of pre-ribosomes in the nucleolus, the release of these factors between State NE1 and State NE2, and subsequent compaction of rRNA may play a significant role in the release of pre-60S particles from the nucleolus (Figure 1B) (4,6).

Last, during the transition between State NE2 and Nog2 State 1, a majority of the remaining rRNA of domain IV stabilizes (Figure 1C). Here, the rRNA chaperone Puf6 is thought to support the accommodation of eL43 by directly binding to eL43 (18,19). Alternatively, Puf6 has been shown to support the stabilization of H68 within rRNA domain IV by facilitating its interaction with H22 and H88 (20,21). In addition, the Rpf2 subcomplex, which includes two RiBi factors Rpf2 and Rrs1 plus the 5S ribonucleoprotein (5S RNP) that contains 5S rRNA as well as the RPs uL18 and uL5, becomes stably anchored onto the pre-LSU together with H80-88 of rRNA domain V (Figure 1C) (14,15). Simultaneously, the RiBi factors Arx1, Rsa4 and Nog2, which are required for rotation of the 5S RNP during late steps of assembly in the nucleoplasm, bind to pre-LSUs (22–24).

To determine which of these four structures, or intermediates between these structures, represents the last nucleolar pre-LSU intermediate in yeast, we studied four proteins, Puf6, uL2, eL43 and Nog2, that either stably anchor onto pre-LSUs in these states or that function during this interval (12,13,15,19,20,25) (Figure 1). We hypothesized that the absence of Puf6, uL2, eL43 or Nog2 might stall ribosome biogenesis during the final stages of nucleolar release. Assays of pre-rRNA processing and pre-LSU constituents in these mutants revealed that shifting the cold-sensitive *puf6Δ* mutant to 13°C inhibits ribosome biogenesis between State NE1 and State NE2. Depletions of uL2, eL43 and Nog2 cause ribosome biogenesis to stall earlier, between Nsa1 State E and State NE1. Importantly, all four of these mutants accumulated pre-LSUs in the nucleolus. Taken together, our data suggest that the last nucleolar intermediate in the assembly of LSUs is likely a structure that is intermediate between State NE1 and State NE2. Our biochemical data suggest that the release of the rRNA steric hinderance factors Nip7, Nop2 and Spb1 is an important trigger for the release of pre-LSUs from the nucleolus.

Materials and methods

Growth of yeast strains

Growth and handling of yeast strains and preparation of standard media were performed by established procedures (26). Rich medium (1% yeast extract, 2% peptone; YEP) or synthetic complete minimal medium (0.15% yeast nitrogen base, 0.5% ammonium sulfate; SC) were supplemented with the ap-

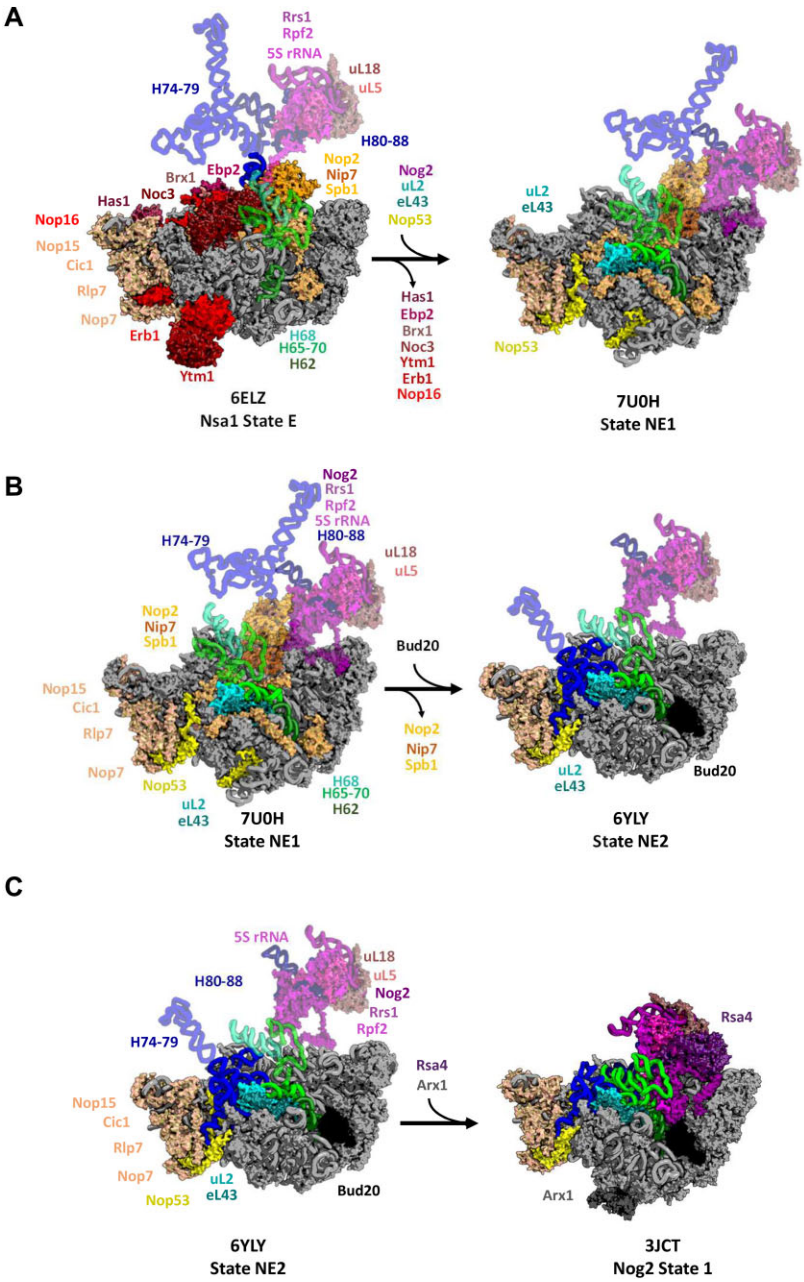

Figure 1. Pre-LSUs undergo numerous protein and rRNA remodeling events as they are released from the nucleolus. Four structures represent the transition of pre-LSUs out of the nucleolus, Nsa1 State E (PDB code 6ELZ), State NE1 (PDB code 7U0H), State NE2 (PDB code 6YLY), and Nog2 State 1 (PDB code 3JCT). Protein and rRNA structures known to be in a structurally heterogeneous state in each of these structures have been overlaid (50% transparency). (**A**) Between Nsa1 State E and State NE1, many nucleolar RiBi factors are released from the maturing large subunit (Ebp2, Brx1, Noc3, Nop16, Erb1, Ytm1 and Has1), the RiBi factors Nog2 and Nop53 bind, and RPs uL2 and eL43 stabilize onto pre-ribosomes. In addition, the rRNA helices H65-70 begin to stabilize and H62 stabilizes. (**B**) The RiBi factors Nip7, Nop2, and Spb1 are released between State NE1 and State NE2. These RiBi factors sterically hinder the stabilization of multiple portions of rRNA domains IV and V onto the pre-LSU. Thus, release of these three RiBi factors may allow rRNA helices H65-70 and H74-79 to stabilize further. At this time, the RiBi factor Bud20 associates with the nascent large subunit. (**C**) Between State NE2 and Nog2 State1, a majority of the remaining rRNA of domains IV and V, as well as 5S rRNA, stabilize onto the large subunit precursor. In addition, many RiBi factors stabilize onto the pre-LSU, including Arx1, Rrs1, Rpf2, Cgr1, Rsa4 and Nog2.

propriate amino acids and bases as nutritional requirements, and with 2% galactose (YEPGal and SC + Gal, respectively), or 2% glucose (YEPGlu and SC + Glu, respectively). All solid media contained 2% agar. Unless otherwise indicated, yeast cells were grown at 30°C to an optical density at 600 nm (OD_{600}) of 0.9.

puf6Δ strains were grown in YEPGlu medium (2% dextrose, 2% peptone, and 1% yeast extract) at 30°C for 15 h and shifted to 13°C for eight hours. *puf6Δ* strains containing plasmids from the Yeast Genomic Tiling Library were grown in selective media (SC-leu + Glu).

GAL-RPL2 and *GAL-RPL43* strains were grown in YEPGal (2% galactose, 2% peptone and 1% yeast extract) at 30°C for 17 h and shifted to YEPGlu (2% dextrose, 2% peptone and 1% yeast extract) for three hours. RP depletion strains containing plasmids used for microscopy were grown in YEPGal

overnight and shifted to YEPGlu for 3 hours or were back-diluted in YEPGal for three hours.

Strains and microbiological methods

All yeast strains used in this work are listed in Supplementary Table S1. The *puf6Δ* strains were generated by PCR-based gene deletion-disruption of the *PUF6* gene in BY4741 or JWY12462 (*TAP-FLAG-NOP53)*. To this end, we amplified either the *PUF6::kanMX6* disruption cassette using the plasmid pFA6a-kanMX6 or *PUF6::HISMX6* using the plasmid pFA6a-HIS3MX6 as templates (Supplementary Table S2) (26). The respective PCR products were transformed into the respective strains by the lithium acetate method (27). Transformants were selected on YEPGlu medium containing 200 μg/ml G418 or SC-his medium. Candidates were chosen and the integration was verified by colony PCR.

To generate the Nop7-TAP tagged strains, the stop codon of *NOP7* was replaced by the TAP sequence in frame. The plasmids pFA6a-TAP-kanMX6 and pFA6a-TAP-TRP1 were used as templates (28). The PCR product was purified and transformed into *puf6Δ, GAL-RPL2* and *GAL-RPL43* strains. The presence of the C-terminal tag was confirmed by western blotting using a monoclonal anti-TAP antibody. The TAP-FLAG-Nop53 strains were generated as described previously (29).

Strains expressing the uL2-Myc or eL43-Myc protein were generated by replacing the stop codon of *RPL2A* or *RPL43B* with the 13-Myc sequence in frame. The plasmid pFA6a-13Myc-kanMX6 was used to amplify the 13-Myc tag and sequences immediately upstream or downstream of the stop codon of the *RPL2* or *RPL43* ORF (Supplementary Table S2) (26). The PCR product was purified and transformed into the strains. Candidates were selected on YEPGlu or YEPGal media containing 200 μg/ml G418. The expression of the tagged protein was confirmed by western blotting using a monoclonal anti-Myc antibody (clone 9E10, Sigma-Aldrich).

puf6Δ and *puf6Δ* Nop7-TAP strains over-expressing various ORFs were generated by transforming plasmids from the Yeast Genomic Tiling Library (30). Candidates were selected on SC-leu media. As a control, the empty vector pRS315 was also transformed into the strains (31).

Affinity purifications of assembling large subunits

Magnetic Dynabeads (Thermo Fisher Scientific) were used to affinity purify large subunit assembly intermediates using TAP-FLAG-Nop53 or Nop7-TAP. TAP-FLAG-Nop53 (500 ml) and Nop7-TAP (150 ml) cultures were grown either in galactose- or glucose-containing liquid media to an OD_{600} of 0.7–0.9. Cells were collected and resuspended in 3.5 ml of Lysis Buffer (50 mM Tris–HCl pH 7.5, 150 mM NaCl, 10 mM $MgCl_2$, 0.075% detergent octyl-phenoxypolyethoxyethanol), and subjected to vortexing with glass beads (0.5 mm diameter, Biospec Products) eight times for 30 s, with incubation on ice in between vortexing. Extracts were clarified by centrifugation and bound to IgG-coated Dynabeads at 4°C for 1 h. Beads were washed three times with the Lysis Buffer and pre-LSUs were eluted by cleaving the TEV protease site within the TAP-tag, using 1–2 μl of TEV Protease (Thermo Fisher Scientific). Proteins were precipitated with 10% trichloroacetic acid (TCA), resuspended in SDS sample buffer and separated by SDS-PAGE on 4–20% Tris-Glycine Novex gels (Thermo Fisher Scientific) followed by silver staining using standard methods.

Western blot analysis

Proteins from whole-cell extracts or from purified pre-LSUs were separated by SDS-PAGE, transferred to an Amersham Protran-supported 0.45 μm nitrocellulose membrane (GE Healthcare Life Sciences), and assayed by western blot analysis. To conserve antiserum by using a lower volume of blotting buffer, and to enable detection of multiple proteins on one blot, membranes were cut into smaller sections based on the known mobility of the different proteins. As Nog2 co-migrates with IgG on 4–20% Tris-Glycine Novex gels, NuPage 4–12% Bis-Tris gels (Thermo Fisher Scientific) were used to assay Nog2 protein by western blotting. TAP-tagged proteins were detected using alkaline phosphatase conjugated to IgG (Pierce). HA-tagged proteins were identified with mouse monoclonal antibody 12CA5 (Thermo Fisher Scientific), and Myc-tagged proteins with 9E10 antibody (Sigma-Aldrich). FLAG-tagged proteins were probed using an ANTI-FLAG M2 monoclonal antibody (Sigma-Aldrich). Otherwise, antibodies specific for RPs or RiBi Factors were used. Alkaline-phosphatase-conjugated anti-mouse or anti-rabbit secondary antibodies (Promega) were used, and colorimetric detection was performed using NBT and BCIP (Promega).

Analysis of pre-60S r-subunits by semi-quantitative mass spectrometry (iTRAQ)

For semi-quantitative mass spectrometry (iTRAQ), pre-LSUs were purified as described above, with the following modifications. 1L cultures were collected for Nop7-TAP purified samples and 2 L cultures were collected for TAP-FLAG-Nop53 purified cultures. Cell pellets were resuspended in TNM150 buffer (50 mM Tris–HCl pH 7.5, 150 mM NaCl, 1.5 mM $MgCl_2$, 0.1% NP-40 and 5 mM 2-mercaptoethanol (Sigma-Aldrich)). After incubation of the lysates with IgG-coated Dynabeads for 1 h at 4°C, NP-40 was omitted from the buffer for all later steps. Purified samples were sent to the Penn State Hershey Core Research Facilities for trypsin digestion and 8-plex labeling with iTRAQ reagents 113, 114, 115, 116, 117, 118, 119 and 121 (Applied Biosystems). Peptides were separated by two-dimensional (2D) liquid chromatography and parent ions were identified on a Sciex 5600 liquid chromatography mass spectrometer system. Protein Pilot 5.0 was used to obtain iTRAQ ratios as an average of all peptides for each protein. Proteins identified with >99.9% confidence were used for further data analysis. Data were normalized to the change in ratio of the bait protein.

Northern blotting and primer extension of pre-rRNA

Steady-state levels of pre-rRNAs were assayed using northern blot and primer extension analysis. Ten milliliter cultures of cells were harvested, frozen, and RNA was extracted using phenol. Five micrograms of RNA were used for primer extension reactions or loaded onto a formaldehyde/MOPS agarose gel for Northern blotting. ^{32}P-γ-ATP radiolabeled oligonucleotide probes for specific pre-rRNAs were used in primer extension reactions and for hybridization in Northern blots. For Northern hybridization of small molecular weight RNAs (7, 6, 5.8 and 5S), RNA samples were mixed with an equal volume of sample buffer (0.1 × TBE buffer, 10M urea, 0.1% xylene cyanol, 0.1% bromophenol blue) and subjected to electrophoresis on a 5% acrylamide/7M urea gel for 4 h at 120 mA. Following electrophoresis, gels were electroblotted to a Nytran N membrane (GE Healthcare Life Sciences) using a

Trans-Blot Plus Cell (Biorad), hybridized with an end-labeled oligonucleotide, washed, and exposed to X-ray film. Oligonucleotide probes or primers are described in Horsey *et al.* (32).

Fluorescence microscopy

Strains were transformed with either plasmid pRS316-uL23-eGFP-mRFP-NOP1, pRS316-NOP7-eGFP-mRFP-NOP1 or pRS316-eGFP-NOP53-mRFP-NOP1 (Supplementary Table S2) and grown in YEPGlu or YEPGal media at indicated temperatures as described previously (see above) (33,34). Cells were fixed in 4% paraformaldehyde for 15 minutes and washed three times in PBS before anchoring to glass slides using 20–30 μl of 1 mg/ml concanavalin A (ConA, Fisher Scientific), which was dried on plates for 30–45 min before adding cells. Cell images were obtained by a Zeiss LSM 880 laser scanning confocal microscope at 1000x magnification. Images were acquired using ZEN software (blue edition, by Zeiss) and the images were processed using Fiji for Mac OSX (National Institutes of Health).

High-copy suppression and enhancer screen

High-copy (two micron) plasmids from the Yeast Genomic Tiling Collection (Open Bio-systems) were transformed into *puf6Δ*, *puf6Δ* Nop7-TAP, Nop7-TAP and BY4741 (*PUF6*) strains (30). Plasmids used can be found in Supplementary Table S2. Serial dilutions of cells (1:10 to 1:10,000) were spotted onto SC-leu + Glu solid medium and incubated at 30°C and 13°C.

Sucrose gradient centrifugation

Cell extracts for polysome profile analyses were prepared as described previously (35). Ten A_{260} units of total cell extract were loaded onto 7–50% sucrose gradients. These gradients were centrifuged at 39,000 rpm in a Beckman Coulter SW41 Ti rotor at 4°C for 2 h 45 min and fractionated using an ISCO UA-6 system with continuous monitoring at A_{254}.

Results

Deletion of *PUF6* blocks LSU biogenesis during late nucleolar stages

To characterize the defects in ribosome biogenesis caused by shifting the cold-sensitive *puf6Δ* mutant to 13°C, we affinity purified pre-LSUs. We initially used the RiBi factor Nop7 as a bait, because it is associated with most nuclear LSU assembly intermediates and can be used to identify the approximate interval of ribosome biogenesis that was inhibited in this mutant (29,36,37) (Supplementary Figure S2D). In the absence of Puf6 at 13°C, we found increased amounts of Nop2, one of the three rRNA steric hindrance factors (Nip7, Nop2 and Spb1), present in pre-LSUs (Supplementary Figures S2 and S3). In contrast, the levels of many strictly nucleolar RiBi factors (Brx1, Has1, Noc2 and Noc3) decreased (Supplementary Figure S2).

We next transitioned to using Nop53 as bait, because it captures a narrower set of intermediates, between State E and Nog2-TAP State 1 (15). Thus, we could observe stronger effects when surveying this smaller interval of assembly (Supplementary Figure S2D) (15). We then assayed changes in levels of RPs and RiBi factors in pre-LSUs using iTRAQ mass spectrometry and western blot analysis. In agreement with previous reports, eL43 incorporation into pre-LSUs was inhibited in the absence of Puf6 (Figure 2D and Supplementary Figure S4B) (18,19). However, we found that amounts of uL2 in pre-LSUs did not decrease in the *puf6Δ* mutant at 13°C (Figure 2D and Supplementary Figure S4B). We found that the levels of Nip7, Nop2 and Spb1 all increased in our second ITRAQ analysis and confirmed again that the levels of Nop2 increased by western blot analysis. Furthermore, we observed that the levels of Has1, Noc2, Noc3, Nop16, Spb4, Ebp2, Brx1, Ytm1 and Erb1 decreased or were unaffected by ITRAQ analysis and western blot analysis (Figure 2 and Supplementary Figure S4B). This suggests that the block in pre-LSU maturation in the *puf6Δ* mutant is stalled upstream of the release of Nip7, Nop2 and Spb1, specifically between State NE1 and State NE2. Because the rRNA steric hindrance factors are not released in the absence of Puf6, a majority of rRNA domains IV and V likely cannot compact onto the body of these pre-LSUs (Figure 1B) (12,15).

Consistent with a block between State NE1 and State NE2, we observe that steps downstream of this transition appear to be blocked. Amounts of Nog2 associated with pre-LSUs decreased, suggesting that Nog2 binding is inhibited (Figure 2, Supplementary Figures S2A and 4B). The levels of Rpf2, Rrs1 and Cgr1 increased when *PUF6* was deleted, indicating that they can bind, but not release from pre-LSUs (Figure 2A). Because these three RiBi factors sterically hinder 5S RNP rotation, this remodeling step most likely does not occur (22,35,38). As the ITS2 spacer RNA is processed, the RiBi factors that are directly bound to it, the ITS2 associated RiBi factors Cic1, Nop15, Nop7 and Rlp7, are released (29,39,40). The levels of these ITS2 associated factors in pre-LSUs increased when *PUF6* was deleted, indicating that their release is inhibited, likely because ITS2 processing does not occur (Figure 2A). Normally, ITS2 removal is thought to occur during the lifetime of the Nog2 particle, consistent with our observed block (14). However, it should be noted that we and others have shown that 5S RNP rotation and ITS2 processing can occur independently of each other (16,29,35,38,40–42). Taken together, these results indicate that Puf6 is required for the transition from state NE1 to state NE2.

Depletion of uL2 or eL43 blocks LSU biogenesis upstream of the *puf6Δ* mutant

Next, we examined the effects on pre-LSU composition caused by depletion of RPs uL2 or eL43. To do so, we purified pre-LSUs using TAP-tagged Nop7 and assayed constituents of pre-LSUs, as described above. The effects on protein constituents of pre-LSUs were very similar when either uL2 or eL43 was depleted (Supplementary Figure S2) (25). The levels of Nop2 and Nip7 increased, while amounts of Erb1, Has1, Noc2 and Noc3 appeared to decrease.

As with the previous assays of the effects of the *puf6* mutant, we next studied the effect of depleting uL2 by ITRAQ analysis using Nop53 as bait to obtain a more detailed understanding of this mutant phenotype. As observed upon deletion of *PUF6*, the levels of the rRNA steric hindrance factors Nip7, Nop2 and Spb1 consistently increased when uL2 was depleted, as previously described (Figure 3 and Supplementary Figures S3 and S4D) (25). The levels of most other nucleolar RiBi factors either did not change or decreased. However, in contrast to results with Nop7-TAP as bait, we observed that amounts of Nop7, Erb1, Ytm1, and Has1 generally increased

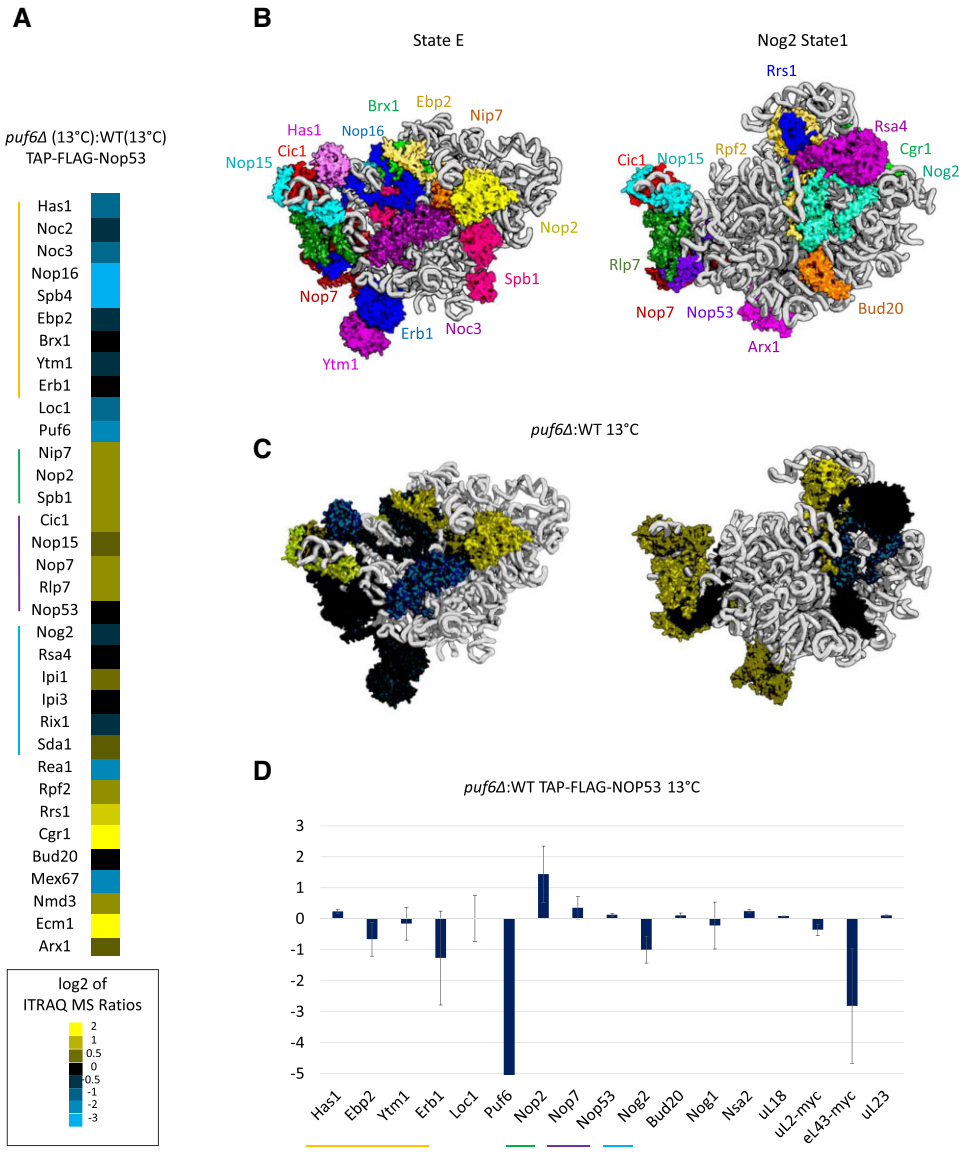

Figure 2. The absence of Puf6 at low temperatures inhibits ribosome biogenesis between State NE1 and State NE2. (**A**) iTRAQ (semi-quantitative mass spectrometry) was used to quantify relative changes in levels of RiBi factors between mutant and wild-type pre-ribosomes. The cold-sensitive *puf6Δ* strain was grown for fifteen hours in YEPGlu medium at 30°C, shifted to 13°C for three hours, and compared with the wild-type *PUF6* strain grown in the same conditions. Ratios of RiBi factors were normalized to levels of Nop53 (bait). Protein groups are marked as follows: Strictly nucleolar RiBi factors, excluding Nip7, Nop2, and Spb1 (orange), rRNA steric hinderance factors (green), ITS2 associated factors (purple), 5S RNP rotation factors (blue). (**B**) Cryo-EM models depicting proteins that were detected by ITRAQ MS. Left: Nsa1 State E with associated RiBi factors. Right: Nog2 State 1 with associated RiBi factors. The colors of the different assembly factors shown are meant to distinguish the assembly factors from each other. These colors are not related to the different classes of factors described in (A). (**C**) Summary of TAP-FLAG-NOP53 ITRAQ MS data for the *puf6Δ* mutant presented on the cryo-EM models in B. Proteins are colored according to log2 ratios found in (A). (**D**) Quantification of western blot assays of *puf6Δ* pre-ribosomes. Samples were collected as described in (A) using Nop53 as bait. Protein constituents were separated by SDS-PAGE and stained with silver, then subjected to western blotting using antibodies against specific proteins. All proteins were analyzed in duplicate. Protein levels were normalized to the levels of Nop53 or uL23. Protein groups are marked with colored bars, as described in (A).

in Nop53-containing particles when uL2 or eL43 were depleted (Figure 3D and Supplementary Figure S4D). We hypothesize that because Nop7, Erb1, Has1 and Ytm1 all associate with the pre-60S from the earliest stages of assembly, a delay or inhibition of their removal was difficult to detect when Nop7 is utilized as a bait. This accumulation of Erb1, Ytm1, and Has1, as well as the rRNA steric hindrance factors Nop2, Nip7 and Spb1, indicates that pre-LSUs cannot complete the transition from Nsa1 State E to State NE1 when either uL2 or eL43 are depleted (Figure 1A).

Depletions of uL2 and eL43 also exhibited downstream defects in assembly that are consistent with a Nsa1 State E to State NE1 block. Similar to the defect observed in the *puf6Δ* mutant, the levels of Nog2 and Bud20 decreased, indicating that their assembly is partially inhibited (Figure 3 and Supplementary Figure S4D) (25). The levels of Rpf2, Rrs1 and Cgr1 increased, indicating that they are not efficiently released from pre-ribosomes, thus preventing rotation of the 5S RNP (Figure 3A). We also observed that the levels of the ITS2 associated factors increased, indicating that the processing of the ITS2

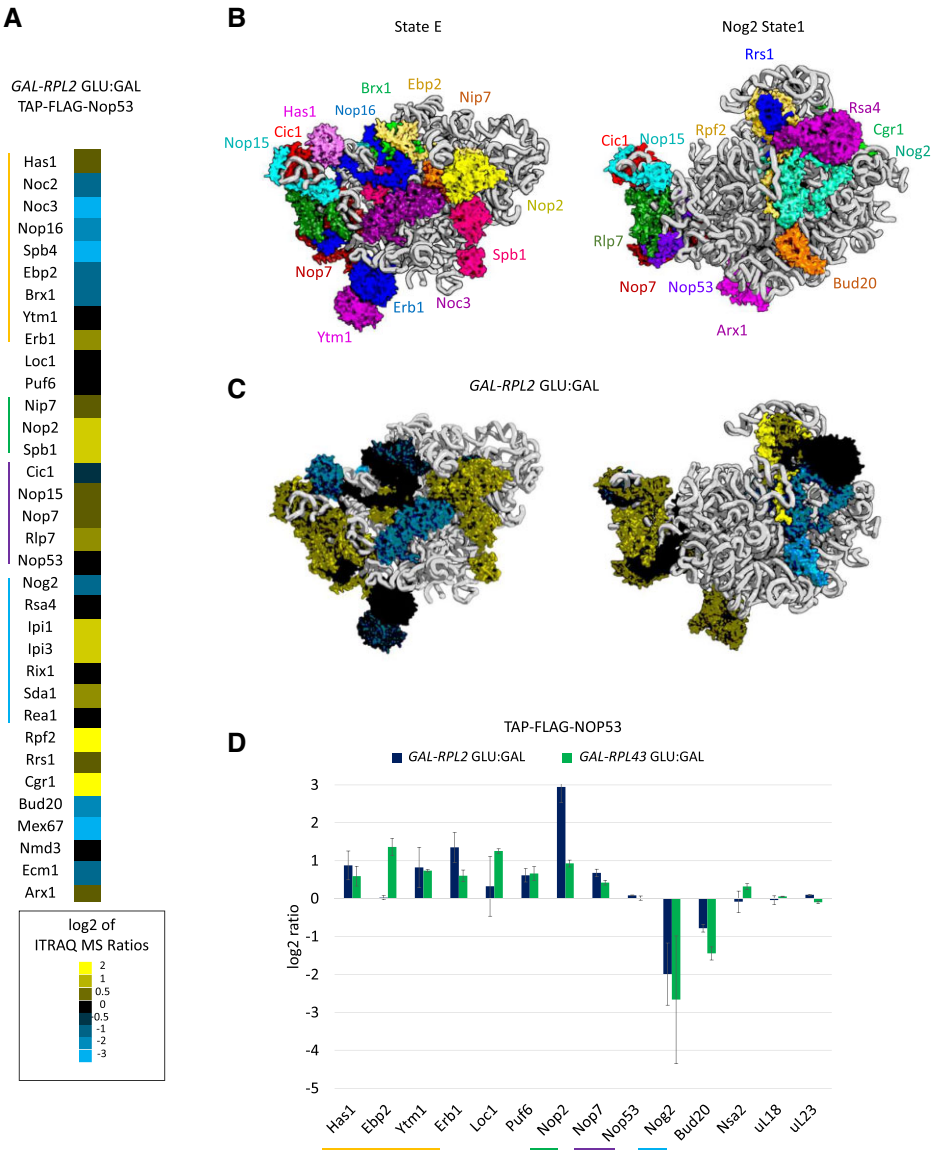

Figure 3. The absence of uL2 or eL43 inhibits ribosome biogenesis between State E and State NE1. (**A**) iTRAQ (semi-quantitative mass spectrometry) was used to quantify relative changes in levels of RiBi factors in pre-ribosomes upon depletion of uL2. The *GAL-RPL2* strain was grown for fifteen hours in YEPGal medium at 30°C, shifted to YEPGlu for three hours to deplete the ribosomal protein uL2, and compared to a non-shifted culture. Ratios of RiBi factors were normalized to levels of Nop53 (bait). Protein groups are marked as follows: Strictly nucleolar RiBi factors, excluding Nip7, Nop2 and Spb1 (orange), rRNA steric hinderance factors (green), ITS2 associated factors (purple), 5S RNP rotation factors (blue). (**B**) Cryo-EM models depicting proteins that were detected by ITRAQ MS. Left: Nsa1 State E with associated RiBi factors. Right: Nog2 State 1 with associated RiBi factors. The colors of the different assembly factors shown are meant to distinguish the assembly factors from each other. These colors are not related to the different classes of factors described in (A). (**C**) Summary of TAP-FLAG-NOP53 ITRAQ MS data for the *GAL-RPL2* mutant presented on the cryo-EM models in B. Proteins are colored according to log2 ratios found in (A). (**D**) Western blot quantification of changes in pre-ribosomal proteins upon depletion of the proteins uL2 or eL43 (*GAL-RPL2* and *GAL-RPL43* strains respectively). Samples for both strains were collected as described in (A) using Nop53 as bait. Protein constituents were separated by SDS-PAGE and stained with silver, then subjected to western blotting using antibodies against specific proteins. All proteins were analyzed in duplicate. Protein levels were normalized to the levels of Nop53 or uL23. Protein groups are marked as described in (A).

spacer RNA is inhibited (Figure 3, Supplementary Figures S2A and S4D).

Taken together, these experiments indicate that uL2 and eL43 are required for release of Erb1, Ytm1, Has1 and the later release of rRNA steric hindrance factors Nip7, Nop2, and Spb1. Thus, depletion of either of these RPs results in a block in pre-LSU biogenesis during the transition from Nsa1 State E to State NE1 (Figure 1A). As a result of this block, downstream assembly events are also inhibited.

Depletion of Nog2 causes a similar, but stronger defect than depletion of either uL2 or eL43

To characterize how ribosome assembly is affected in the absence of Nog2, we performed iTRAQ mass spectrometry and western blot analysis of pre-LSUs that were affinity-purified with TAP-tagged Nop53 when Nog2 was depleted. Our data suggest that the levels of the rRNA steric hindrance factors Nip7, Nop2, and Spb1, as well as Erb1, Ytm1, Has1 and Nop7 increase (Figure 4, Supplementary Figures S3 and S4F). This

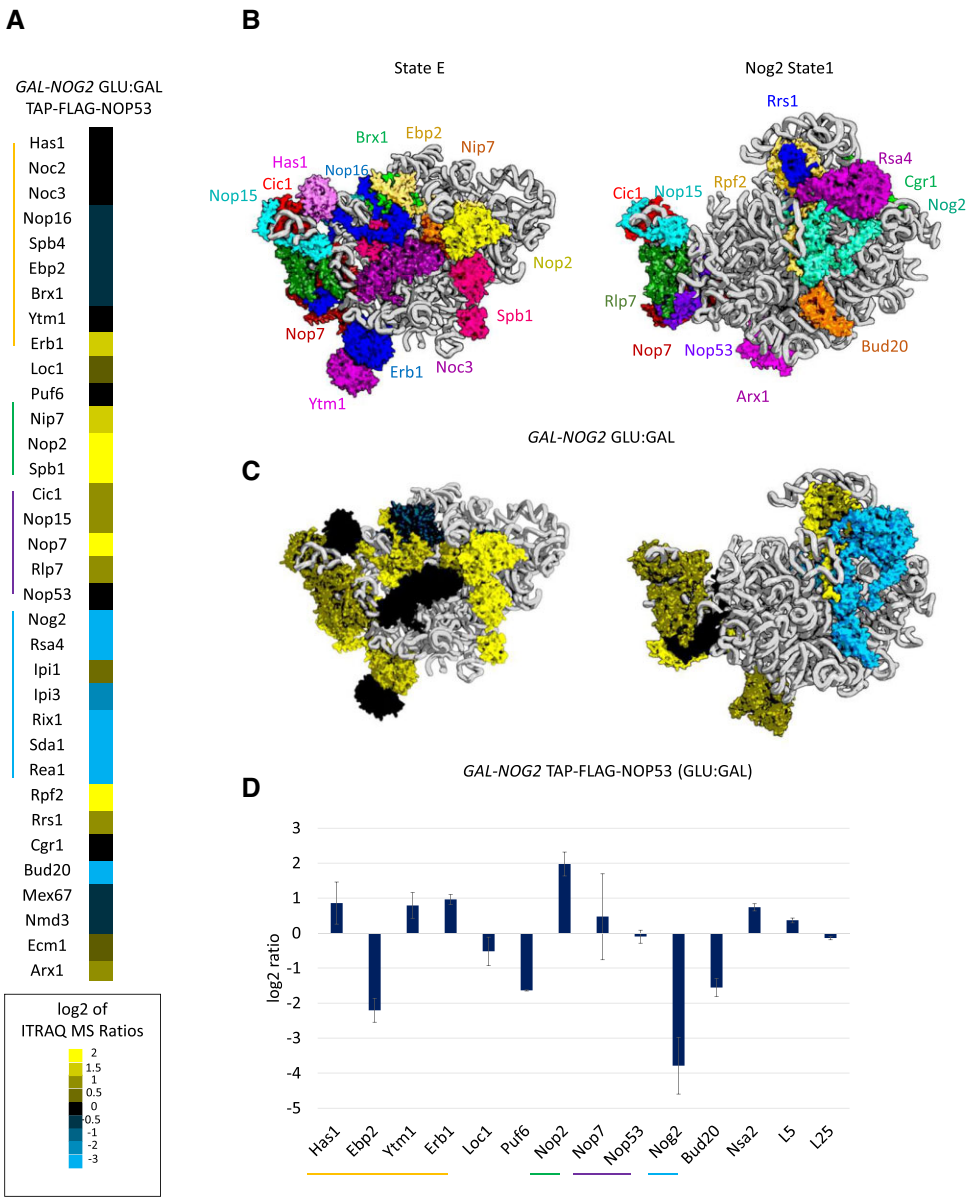

Figure 4. Depletion of Nog2 results in a block in ribosome biogenesis between State E and State NE1. (**A**) iTRAQ (semi-quantitative mass spectrometry) was used to quantify relative changes in levels of RiBi factors in pre-ribosomes upon depletion of Nog2. The *GAL-NOG2* strains were grown for 15 h in YEPGal medium at 30°C, shifted to YEPGlu for three hours to deplete Nog2, and compared to a non-shifted culture. Ratios of RiBi factors were normalized to levels of Nop53 (bait). Protein groups are marked as follows: Strictly nucleolar RiBi factors, excluding Nip7, Nop2 and Spb1 (orange), rRNA steric hinderance factors (green), ITS2 associated factors (purple), 5S RNP rotation factors (blue). (**B**) Cryo-EM models depicting proteins that were detected by ITRAQ MS. Left: Nsa1 State E with associated RiBi factors. Right: Nog2 State 1 with associated RiBi factors. The colors of the different assembly factors shown are meant to distinguish the assembly factors from each other. These colors are not related to the different classes of factors described in (A). (**C**) Summary of TAP-FLAG-NOP53 ITRAQ MS data for the *GAL-NOG2* mutant presented on the cryo-EM models in B. Proteins are colored according to log2 ratios found in (A). (**D**) Western blot quantification of changes in pre-ribosomal proteins upon depletion of Nog2. Samples were collected as described in (A) using Nop53 as bait. Protein constituents were separated by SDS-PAGE and stained with silver, then subjected to western blotting using antibodies against specific proteins. All proteins were analyzed in duplicate. Protein levels were normalized to Nop53 or uL23. Protein groups are marked as described in (A).

latter effect on the transition from State E to NE1 suggests that Nog2 is associated with pre-ribosomes earlier than previously thought (see Discussion).

Like the other mutants examined here, the ITS2 associated factors as well as Rpf2 and Rrs1 accumulated in pre-LSUs when Nog2 was depleted (Figure 4A). This indicates that rotation of the 5S RNP and ITS2 processing are inhibited. In contrast to depletions of uL2 or deletion of Puf6, depletion of Nog2 caused the levels of the RiBi factors Rsa4, Ipi3, Rix1, Sda1 and Rea1 to decrease dramatically in TAP-Nop53 purified pre-LSUs (Figure 4A). This effect was more significant than what we observed for depletion of uL2 or for the *puf6Δ* mutant (Figures 2A, 3A and 4A). Prior to rotation of the 5S RNP, these RiBi factors must bind to pre-LSUs (23,43). The decreased levels of these proteins indicate that they cannot bind to pre-LSUs when Nog2 is depleted.

Pre-rRNA processing defects indicate that uL2 and eL43 mutants stall assembly earlier than *puf6Δ* mutants, and that depletion of Nog2 stalls assembly at two points

We next systematically examined pre-rRNA processing defects of these four mutants by Northern blotting and primer extension. When the cold-sensitive *puf6Δ* mutant was shifted from 30°C to 13°C for three hours, 7S pre-rRNA accumulated, indicating that cleavage of the ITS2 spacer at the C_2 site can occur, but subsequent processing of ITS2 is inhibited (Supplementary Figures S1 and S5A). We observed accumulation of 27SB and $27SA_2$ pre-rRNAs, and decreased levels of 7S pre-rRNA when uL2 or eL43 were depleted for three hours (Supplementary Figure S5B). Accumulation of small amounts of $27SA_2$ pre-rRNA often occurs when this interval of pre-ribosome maturation is blocked, likely due to sequestration in the aborted particles of small amounts of RiBi factors required for very early stages of assembly (44,45). Consequently, we suspect that this is an indirect effect. Thus, we confirmed that when uL2 or eL43 are absent, pre-rRNA processing is blocked before cleavage of ITS2 at the C_2 site (Supplementary Figures S1 and S5B) (25).

Yeast depleted of Nog2 accumulate both 27SB and 7S pre-rRNAs, as previously reported (Supplementary Figure S5C) (13). This may indicate that ribosome biogenesis is stalled at two steps when Nog2 is depleted. The accumulation of 27SB pre-rRNAs likely reflects the population of pre-LSUs that are stalled between Nsa1 State E and State NE1, similar to depletions of uL2 or eL43. On the other hand, the accumulation of 7S pre-rRNAs may reflect the pool of pre-LSUs that are stalled at a later stage (See Discussion). It remains to be determined why some of these Nog2-depleted cells are able to undergo cleavage at the C_2 site within ITS2, while others are not. The defects in pre-rRNA processing in each of these mutants are unlikely to be a result of a shift in the carbon source, as this has been shown to not affect the relative amounts of pre-rRNA processing intermediates (46).

Puf6, uL2, eL43 and Nog2 are required for release of pre-LSUs from the nucleolus

We next assayed whether blocking assembly between Nsa1 State E and State NE1 upon uL2, eL43 or Nog2 depletion or between State NE1 and State NE2 in the *puf6Δ* mutant shifted to 13°C prevented release of pre-LSUs from the nucleolus. To do so, RP uL23-GFP was used as a reporter for pre-LSUs and the RiBi factor mRFP-Nop1 was used as a reporter for the nucleolus. We found that, in each mutant, pre-LSUs localized primarily to the nucleolus, although the effects were weaker in the *puf6Δ* mutant, consistent with the weaker effect on growth (Figure 5). Nucleolar accumulation of pre-LSUs upon Nog2 depletion has been reported in *Drosophila* cells previously (47).

We next assayed the localization of Nop53 in each mutant, to assess effects more specifically on the pre-ribosomes that we affinity-purified using TAP-Nop53 as bait. In wild-type cells Nop53 is localized to both the nucleolus and the nucleoplasm (Supplementary Figure S6). However, in each of the four mutants, there was significant enrichment of GFP-Nop53 in the nucleolus and much less signal in the nucleoplasm, indicating that the pre-ribosomes affinity purified using Nop53 were largely unable to be released from the nucleolus (Supplementary Figure S6).

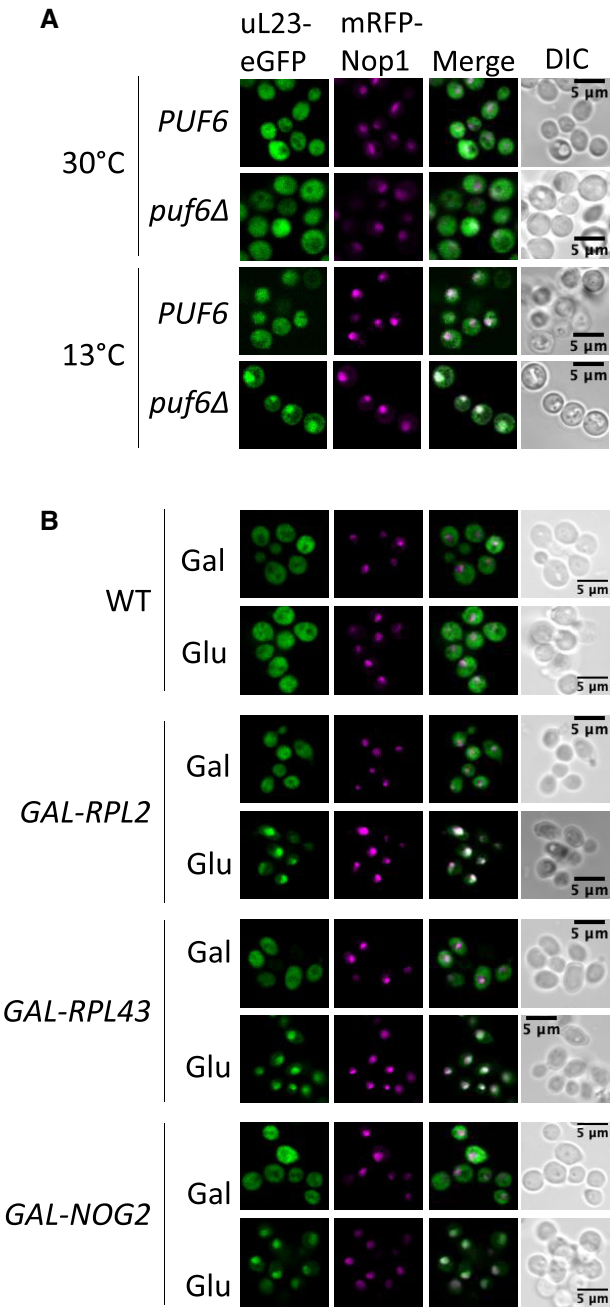

Figure 5. Depletion of uL2, eL43, or deletion of *PUF6* causes nucleolar accumulation of pre-LSUs. The reporter for pre-LSU localization, uL23-eGFP (green), the nucleolar marker mRFP-Nop1 (magenta), the merged signal, and the phase contrast images (DIC) of cells are labeled. Scale bars (marked in black) are 5 μm. Representative images are included. (**A**) The *PUF6* wild-type (BY4741) and *puf6Δ* mutant strains were grown in YEPGlu media for 15 h at 30°C and shifted to 13°C for eight hours. (**B**) *GAL-RPL2*, *GAL-RPL43* and *GAL-NOG2* strains were grown in YEPGal media at 30°C for 15 hours. Glu samples were shifted to YEPGlu media for three hours at 30°C prior to imaging. Gal samples were back diluted to YEPGal media for three hours at 30°C prior to imaging.

Our results indicate that pre-LSUs that are stalled during the transition from State NE1 to State NE2 and accumulate in the *puf6Δ* mutant, localize to the nucleolus. Because the mutant pre-LSU intermediates that accumulate when uL2, eL43 or Nog2 are depleted precede the block caused by a *puf6Δ*, it is not surprising that these depleted strains also accu-

mulate pre-LSUs in the nucleolus. It appears that uL2, eL43, Nog2 and Puf6 are all required for the release of pre-LSUs from the nucleolus, but the function of Puf6 appears to be more proximal to nucleolar release than the function of uL2, eL43 or Nog2.

Since particles that represent intermediates between State NE1 and State NE2 accumulate primarily in the nucleolus, we conclude that these intermediate particles may be the last known nucleolar assembly intermediate of the large subunit.

Increased dosage of *RPL2, RPL43* or *RPL19* suppresses the *puf6Δ* growth defect

The absence of Puf6 causes the last identified block of ribosome biogenesis in the nucleolus. To identify other proteins that might functionally interact with Puf6 during this step, we systematically examined the effect of increased dosage of forty RiBi factor and RP genes that function in LSU biogenesis. To do so, we transformed into a *puf6Δ* strain high copy plasmids expressing these genes from a yeast genomic tiling library, and assessed the effect on growth at 13°C (30).

We found that increased dosage of plasmids containing *RPL2, RPL43*, and *RPL19* suppressed the growth defect of the *puf6Δ* strain, which suggests that these proteins functionally interact with Puf6 (Figure 6A). The growth of wild-type *PUF6* yeast transformed with these plasmids was not affected (Supplementary Figure S7). Increased dosage of the other 37 RiBi factor or RP genes did not visibly affect growth of the *puf6Δ* mutant (Supplementary Figure S8, and data not shown). Suppression of the cold-sensitive growth defect of the *puf6Δ* mutant by increased dosage of *RPL43* has been reported previously (18). It is important to note that the plasmids used in these experiments contain multiple genes, not just those encoding the RPs or RiBi factors on which we focused. However, the most parsimonious explanation for the effects on ribosome biogenesis that we observed when these plasmids were introduced is that the genes related to ribosome biogenesis are being expressed and influence the pathway.

To determine whether increasing the dosage of *RPL2*, *RPL43* and *RPL19* also suppresses the ribosome biogenesis defect of the *puf6Δ* mutant, we analyzed levels of free SSUs and LSUs by sucrose gradient fractionation of lysates from the various *puf6Δ* strains containing high copy plasmids. As expected, the absence of Puf6 caused a deficit of mature LSUs, evident by decreased levels of free LSUs *versus* free SSUs relative to the positive control (Supplementary Figure S9). We found that the ratio of LSUs to SSUs was partially restored only in *puf6Δ* strains containing a plasmid encoding *RPL2* or *RPL19, whereas* increased dosage of *RPL43* had no visible effect on the relative amount of 60S ribosomes (Supplementary Figure S9). These results suggest that suppression of the growth defect by increased dosage of these genes might not markedly improve the efficiency of LSU assembly, but instead might overcome defects in the accuracy of assembly. Similar results have been obtained previously, where multicopy suppressors of RiBi factor mutant growth defects did not increase the amounts of the corresponding ribosomal subunits (48 and references therein).

Increased dosage of *NOG2* supports Nog2 binding onto the *puf6Δ* mutant pre-LSUs

Surprisingly, we found that increased dosage of a plasmid containing *NOG2* exacerbated the cold-sensitive growth defect of the *puf6Δ* mutant (Figure 6A). Importantly, increased dosage of *NOG2* did not cause a growth defect in a wild-type *PUF6* strain, indicating that this exaggerated growth defect is dependent on the absence of Puf6 (Supplementary Figure S7).

The amount of Nog2 associated with pre-LSUs decreases in the *puf6Δ* mutant (Figure 2, Supplementary Figures S2A and S4B) (20). Therefore, we affinity purified pre-LSUs from *puf6Δ* strains that contained plasmids encoding *RPL2, RPL43, RPL19* or *NOG2* to determine whether and how the increased dosage of these genes affects the binding of Nog2 onto nascent LSUs. Intriguingly, in the *puf6Δ* mutant that contained additional copies of the *NOG2* gene, the amount of Nog2 protein associated with purified pre-LSUs *exceeded* wild-type levels (Figure 6C). When this same experiment was replicated in a wild-type *PUF6* background, we found that increased dosage of *NOG2* alone was not sufficient to drive its incorporation into pre-LSUs (Supplementary Figure S10). This indicates that increased dosage of *NOG2* may enable incorporation of Nog2 into pre-LSUs in the absence of Puf6.

Discussion

Here, we identified a candidate for the last nucleolar assembly intermediate of the pre-LSU by studying the effect of depleting uL2, eL43, Nog2 or deleting *PUF6*. We hypothesized that ribosome biogenesis in these four mutants would be inhibited at or near the threshold of nucleolar release, because these proteins might be necessary for compaction and stabilization of rRNA and protein structures in nascent LSUs during this interval (12,15,20). Of these four mutants, we found that the cold-sensitive *puf6Δ* mutant, which is stalled between State NE1 and State NE2 (Figure 7), accumulates the most mature nucleolar ribosome assembly intermediate that has been identified so far.

By focusing on State NE1/State NE2 intermediate particles as the most mature nucleolar pre-LSU thus far identified, we can now assess *how* some pre-ribosomes are released from the nucleolus. What characteristics of State NE1/State NE2 intermediate pre-LSUs cause them to be nucleolar, and how can remodeling these features enable them to be released from the nucleolus? To answer these questions, we can examine the release of pre-ribosomes from the nucleolus from the perspective of the nucleolus as a biomolecular condensate that forms via interactions between pre-ribosomes (5). Both the rRNA and proteins in nascent ribosomes are, in theory, capable of interacting in *trans*. Uncompacted rRNA (rRNA that has not attained mature structure) may readily interact in *trans* with other RNAs, as well as proteins, to support phase separation leading to condensate formation (49–51). Many RiBi factors contain intrinsically disordered regions (IDRs), which are protein sequences predicted to have little or no structure (4,52). IDRs have been shown to support phase separation by interacting in *trans* with both proteins and RNA (10,53–55).

We have observed that nucleolar pre-LSUs and pre-SSUs contain significantly more uncompacted rRNA and IDRs that may facilitate *trans* interactions, compared to nucleoplasmic or cytoplasmic pre-ribosomes (4). Our bioinformatics work (4) and *in vitro* experiments published in Riback *et al.* (6) suggest that, when the number of *trans* interactions drops below a critically low threshold, maturing subunits are released from the nucleolus because they cannot interact sufficiently with other components of the nucleolus. Therefore, we conclude that State NE1/State NE2 intermediate pre-LSUs likely

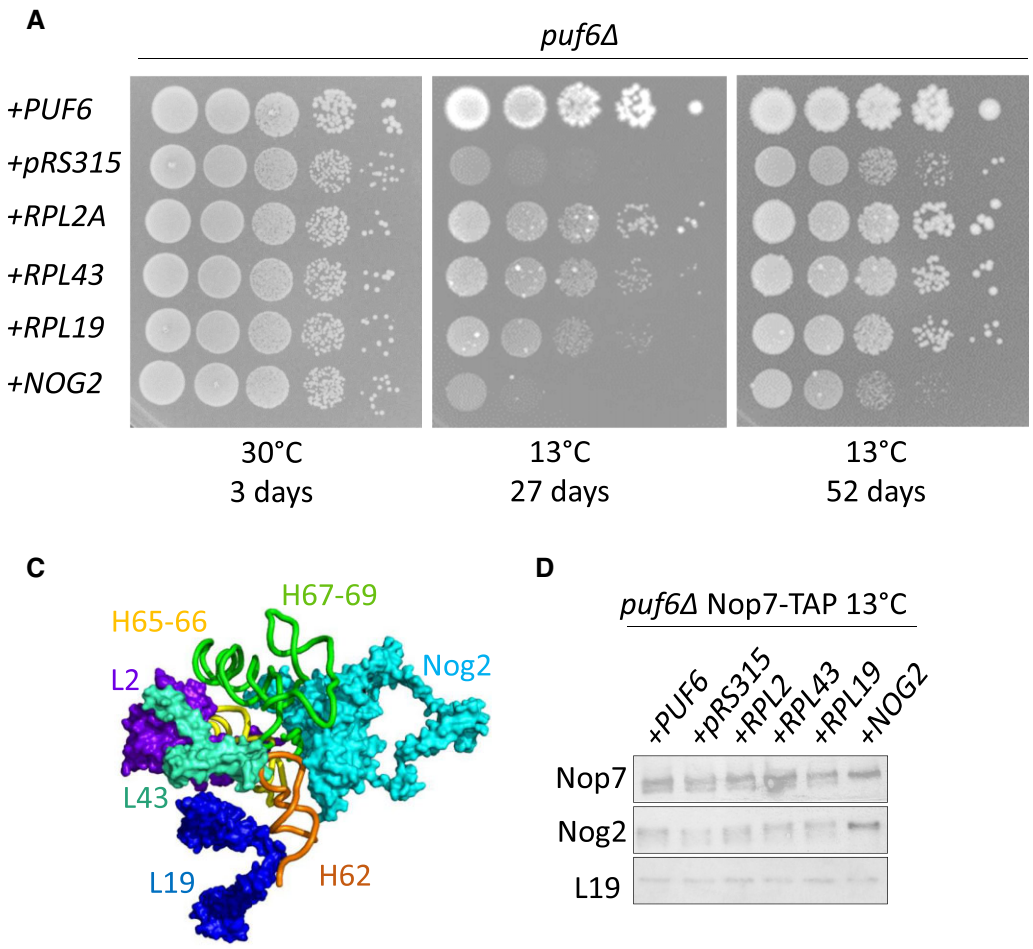

Figure 6. Increased dosage of the *RPL2A, RPL43B,* and *RPL19B* genes suppresses the cold sensitive growth defect of the *puf6Δ* mutant, while over-expression of RiBi factor *NOG2* exacerbates the growth defect. (**A**) Growth of *puf6Δ* strains containing plasmids that carry the *RPL2A, RPL43B, RPL19B,* or *NOG2* genes. Serial dilutions (1:10 to 1:10,000) of these strains were spotted onto C-leu + Glu solid medium and incubated at 30°C and 13°C. (**B**) Model of uL2, eL43, eL19 and Nog2 alongside interconnecting rRNA helices in Nog2 State 1 pre-LSU particles (PDB 3JCT). (**C**) Pre-LSUs were affinity-purified using the RiBi factor Nop7 as a bait. Samples from each strain shown in A were separated by SDS-PAGE and stained with silver (Supplementary Figure S10A). Samples were subjected to western blotting using antibodies against specific proteins. All samples were derived from the same experiment, and western blots were processed in parallel.

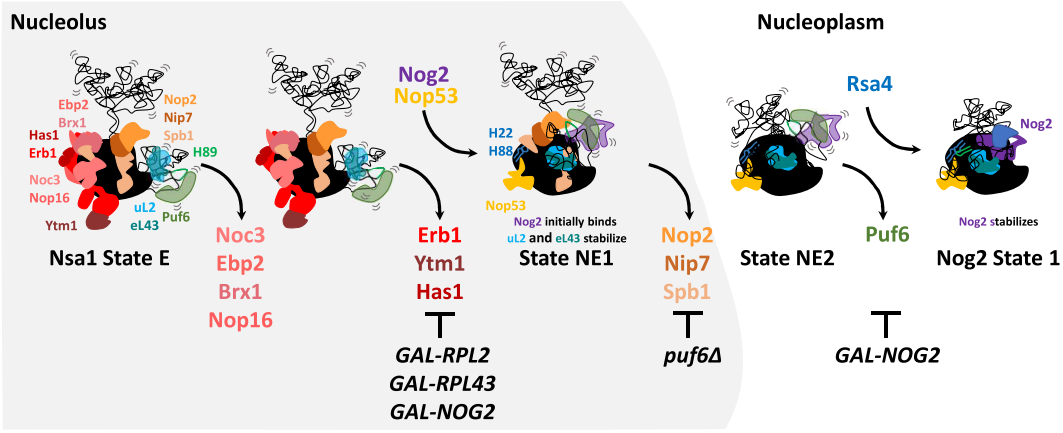

Figure 7. uL2, eL43, Puf6 and Nog2 facilitate the nucleolar release of pre-LSUs. The initial association of ribosomal proteins uL2 and eL43 and RiBi factor Nog2 with noncompacted rRNA in pre-60S ribosomes supports the release of RiBi factors Erb1, Ytm1, and Has1 from the nascent large subunit. Puf6 facilitates the stabilization of eL43 and supports the release of Nip7, Nop2 and Spb1. Thereafter, Puf6 is released and Nog2 stabilizes to form Nog2 State 1 particles. Because pre-ribosomes accumulate in the nucleolus in each of these mutants, it is likely that an intermediate between State NE1 and State NE2 is likely the last known pre-60S subunit in the nucleolus.

are retained in the nucleolus because *trans* interactions above this threshold are maintained. This may be because the presence of the rRNA steric hindrance factors, Nip7, Nop2 and Spb1, inhibits the compaction and stabilization of rRNA domains IV and V. Importantly, these rRNA domains represent about 30% of the rRNA of the pre-LSU, and can therefore contribute significantly to the number of *trans* interactions that pre-LSUs can attain. Furthermore, two out of these three rRNA steric hindrance factors, Nop2 and Spb1, contain IDRs that may also be able to undergo *trans* interactions (4). Ultimately, if the rRNA steric hindrance factors are not released, more *trans* interactions are present and the critically low threshold for *trans* interactions is not reached. Thus, the removal of the rRNA steric hindrance factors from State NE1 particles may be the last, or one of the last, remodeling events that enable pre-LSUs to reach the low threshold of *trans* interactions necessary for their release from the nucleolus.

How might Puf6 enable remodeling of pre-ribosomes to release the steric hindrance factors? Puf6 is present on nascent LSUs from the earliest stages of ribosome biogenesis (Supplementary Figure S11) (19,37). Crosslinking and *in vitro* FRET experiments as well as cryo-EM analysis indicate that Puf6 binds to rRNA helix H68 and functions to stabilize the interaction between H68 and the 'kissing loops', H22 and H88, between State NE2 and Nog2 State 1 (Supplementary Figure S12) (20,21). We confirmed that Puf6 supports the stable incorporation of eL43 after its initial encounter with pre-60S particles (18,19). Puf6 may function through direct contact with eL43, or indirectly through its interaction with rRNA H68 (18–21). This raises a question; why does deletion of *PUF6* cause a different defect than depletion of eL43? We hypothesize that only the stabilization, not the initial binding of eL43 is affected by deletions of Puf6. Therefore, the role of eL43 in the initial recruitment of Nog2, and the subsequent release of Erb1, Ytm1, and Has1, would not be affected by the absence of Puf6. Assembly of uL2 and eL43 onto pre-LSUs may play an active role in the release of Nip7, Nop2 and Spb1. As uL2 and eL43 begin stabilizing onto H74-75, they may support the release of Nip7, Nop2 and Spb1 and, afterward, the stable association of Nog2 onto the pre-LSU. However, when Puf6 is absent at low temperatures, the structure of H68 may be affected. As previously shown, rRNA helices H68 and H74-75 are in close proximity to one another, and defects in one may affect the structure of the other (Supplementary Figure S12) (35). Thus, the absence of Puf6 may cause the formation of aberrant rRNA structures that inhibit the stabilization of eL43 with H74-75, and, as a result, the release of Nip7, Nop2, and Spb1 would be blocked.

Increased dosage of either *RPL2* and *RPL43* suppresses the Cs- phenotype of the *puf6Δ* mutant, consistent with Puf6 enabling the association of uL2 and eL43 with pre-ribosomes. Extra copies of the *RPL19* gene also suppress the growth defect of a *puf6Δ* mutant. Prior to the stabilization of eL43 and uL2, eL19 contacts and co-stabilizes with rRNA helix H62, a component of the binding site for eL43 (Figure 6B) (14,15). Therefore, it is not surprising that increasing the dosage of *RPL19* might support formation of the eL43 binding site and, therefore, indirectly enable eL43 stabilization to suppress the defect of a *puf6Δ* mutant.

In contrast, we observed that increasing the dosage of *NOG2* exacerbates the cold-sensitive growth defect of the *puf6Δ* mutant (Figure 6A). One possible explanation for this phenotype is that rRNA helices H67-70, the rRNAs that form the binding site of both Puf6 and Nog2, may become kinetically trapped in the absence of Puf6 at cold temperatures (14,20,24,56,57). Such a kinetic trap may limit the initial binding of Nog2 onto the assembling LSU. However, increased dosage of *NOG2* might increase the probability that Nog2 binds onto this kinetically trapped, misfolded rRNA and, as a result, the rRNA cannot escape the kinetic trap (Figure 6C).

Interestingly, we found that depletion of Nog2 causes LSU maturation to stall at two points, as evidenced by the accumulation of 27SB and 7S pre-rRNAs (Supplementary Figure S5C). Our microscopy data indicate that Nog2 depletions primarily exhibit nucleolar accumulation (Figure 5B). We postulate that the accumulation of 27SB pre-rRNA upon Nog2 depletion represents a large population of pre-LSUs that are stalled in the nucleolus, between Nsa1 State E and State NE1. This idea is supported by our observation that depletions of uL2 and eL43, which block ribosome biogenesis between Nsa1 State E and State NE1, accumulate only 27SB pre-rRNA and cause pre-ribosomes to localize to the nucleolus (Figure 5B). Association of Nog2 with pre-ribosomes during this early period is supported by recent cryo-EM studies by Cruz *et. al.* who identified a small portion of Nog2 associated with NE1 particles (17, PDB 7UOH). Furthermore, Nog2 begins to assemble into pre-ribosomes at this stage in human pre-60S particles visualized by cryo-EM (58). The presence of Nog2 in yeast pre-ribosomes at this earlier stage is further supported by the copurification of early RiBi factors such as Puf6, Loc1, Erb1, Has1 with pre-LSUs isolated using Nog2 as bait (18,25,41) (Supplementary Figure S11).

However, previous work by Saveanu *et al.* also indicates that pre-ribosomes depleted of Nog2 accumulate in both the nucleolus and the nucleoplasm when assayed by *in situ* hybridization and electron microscopy, a more sensitive assay than fluorescence microscopy that we used (13). We hypothesize that the accumulation of 7S pre-rRNA upon Nog2 depletion suggests the presence of a second population of pre-LSUs that are stalled at a later step downstream during the nucleoplasmic stages of ribosome biogenesis. It likely that this stall occurs at the point in assembly where Nog2 normally stabilizes completely onto pre-LSUs, between State NE2 and Nog2 State 1 (Figure 7) (14). This may explain why the levels of RiBi factors that associate at later stages of ribosome assembly are so strongly affected when Nog2 is depleted but not when uL2 is depleted (Figures 3A and 4A).

In summary, we found that the combined functions of uL2, eL43, Nog2 and Puf6 support the release of pre-LSUs from the nucleolus. We hypothesize that a critically low threshold of *trans* interactions must be reached for pre-ribosomes to undergo nucleolar release. We determined that the decrease in *trans* interactions required for the release of pre-LSU assembly intermediates from the nucleolus is likely reached at an intermediate between State NE1 and State NE2. Our data strongly indicate that the release of Nip7, Nop2 and Spb1 from pre-LSU assembly intermediates, coupled with the compaction and stabilization of *trans*-interacting rRNA domains, is ultimately responsible for the nucleolar release of pre-LSUs. These findings have clarified the mechanisms by which pre-LSUs are released from the nucleolus, which elucidates the relationship between ribosome biogenesis and the nucleolus as a biological condensate.

Data availability

The data that support this work are available from the corresponding authors upon request.

Supplementary data

Supplementary Data are available at NAR Online.

Acknowledgements

We thank Craig Kaplan, Tina Lee, Joel McManus, and the members of our laboratory for critical reading of this manuscript, technical assistance, and helpful discussions. We thank S. Rospert (eL19, eL39), C. Saveanu and M. Fromont-Racine (Tif6, Rlp24, Nsa2), J. Maddock (Nog1), V. Panse (Bud20), P. Linder (Has1), M. McAlear (Ebp2), and K.-Y. Lo (Puf6, Loc1) for antisera, and J. Baβler for providing plasmids containing uL23-eGFP and mRFP-Nop1.

Funding

National Institutes of Health [R01GM028301 to J.L. Woolford, Jr.]. Funding for open access charge: National Institutes of Health [R01GM028301].

Conflict of interest statement

None declared.

This paper is linked to: doi:10.1093/nar/gkac430.

References

1. Klinge,S. and Woolford,J.L. (2019) Ribosome assembly coming into focus. *Nat. Rev. Mol. Cell Biol.*, **20**, 116–131.
2. Woolford,J.L. and Baserga,S.J. (2013) Ribosome biogenesis in the yeast *Saccharomyces cerevisiae*. *Genetics*, **195**, 643–681.
3. Kressler,D., Hurt,E. and Baßler,J. (2010) Driving ribosome assembly. *Biochim. Biophys. Acta - Mol. Cell Res.*, **1803**, 673–683.
4. LaPeruta,A.J., Micic,J. and Woolford,J.L. (2022) Additional principles that govern the release of pre-ribosomes from the nucleolus into the nucleoplasm in yeast. *Nucleic Acids Res.*, https://doi.org/10.1093/nar/gkac430.
5. Lafontaine,D.L.J., Riback,J.A., Bascetin,R. and Brangwynne,C.P. (2020) The nucleolus as a multiphase liquid condensate. *Nat. Rev. Mol. Cell Biol.* **22**:*165-182* .
6. Riback,J.A., Zhu,L., Ferrolino,M.C., Tolbert,M., Mitrea,D.M., Sanders,D.W., Wei,M., Kriwacki,R.W. and Brangwynne,C.P. (2020) Composition-dependent thermodynamics of intracellular phase separation. *Nature*, **581**, 209–214.
7. Oakes,M., Aris,J.P., Brockenbrough,J.S., Wai,H., Vu,L. and Nomura,M. (1998) Mutational analysis of the structure and localization of the nucleolus in the yeast *Saccharomyces cerevisiae*. *J. Cell Biol.*, **143**, 23–34.
8. Oakes,M.L., Johzuka,K., Vu,L., Eliason,K. and Nomura,M. (2006) Expression of rRNA genes and nucleolus formation at ectopic chromosomal sites in the yeast *Saccharomyces cerevisiae*. *Mol. Cell. Biol.*, **26**, 6223–6238.
9. Nicolas,E., Parisot,P., Pinto-Monteiro,C., De Walque,R., De Vleeschouwer,C. and Lafontaine,D.L.J. (2016) Involvement of human ribosomal proteins in nucleolar structure and p53-dependent nucleolar stress. *Nat. Commun.*, **7**, 11390.
10. White,M.R., Mitrea,D.M., Zhang,P., Stanley,C.B., Cassidy,D.E., Nourse,A., Phillips,A.H., Tolbert,M., Taylor,J.P. and Kriwacki,R.W. (2019) C9orf72 Poly(PR) dipeptide repeats disturb biomolecular phase separation and disrupt nucleolar function. *Mol. Cell*, **74**, 713–728.
11. Baßler,J., Kallas,M., Pertschy,B., Ulbrich,C., Thoms,M. and Hurt,E. (2010) The AAA-ATPase rea1 drives removal of biogenesis factors during multiple stages of 60S ribosome assembly. *Mol. Cell*, **38**, 712–721.
12. Kater,L., Thoms,M., Barrio-Garcia,C., Cheng,J., Ismail,S., Ahmed,Y.L., Bange,G., Kressler,D., Berninghausen,O., Sinning,I., *et al.* (2017) Visualizing the assembly pathway of nucleolar Pre-60S ribosomes. *Cell*, **171**, 1599–1610.
13. Saveanu,C., Bienvenu,D., Namane,A., Gleizes,P.E., Gas,N., Jacquier,A. and Fromont-Racine,M. (2001) Nog2p, a putative GTPase associated with pre-60S subunits and required for late 60S maturation steps. *EMBO J.*, **20**, 6475–6484.
14. Wu,S., Tutuncuoglu,B., Yan,K., Brown,H., Zhang,Y., Tan,D., Gamalinda,M., Yuan,Y., Li,Z., Jakovljevic,J., *et al.* (2016) Diverse roles of assembly factors revealed by structures of late nuclear pre-60S ribosomes. *Nature*, **534**, 133–137.
15. Kater,L., Mitterer,V., Thoms,M., Berninghausen,O., Cheng,J., Beckmann,R. and Hurt,E. (2020) Construction of the central protuberance and L1 stalk during 60S subunit biogenesis. *Mol. Cell*, **79**, 615–628.
16. Cepeda,L., Bagatelli,F., Santos,R., Santos,M., Nogueira,F. and Oliveira,C. (2019) The ribosome assembly factor Nop53 controls association of the RNA exosome with pre-60S particles in yeast. *J. Biol. Chem.*, **294**, 19365–19380.
17. Cruz,V.E., Sekulski,K., Peddada,N., Sailer,C., Balasubramanian,S., Weirich,C.S., Stengel,F. and Erzberger,J.P. (2022) Sequence-specific remodeling of a topologically complex RNP substrate by Spb4. *Nat. Struct. Mol. Biol.*, **29**, 1228–1238.
18. Yang,Y.T., Ting,Y.H., Liang,K.J. and Lo,K.Y. (2016) The Roles of Puf6 and Loc1 in 60S Biogenesis are interdependent, and both are required for efficient accommodation of Rpl43. *J. Biol. Chem.*, **291**, 19312–19323.
19. Liang,K.J., Yueh,L.Y., Hsu,N.H., Lai,J.S. and Lo,K.Y. (2019) Puf6 and Loc1 are the dedicated chaperones of ribosomal protein Rpl43 in *Saccharomyces cerevisiae*. *Int. J. Mol. Sci.*, **20**, 5941.
20. Gerhardy,S., Oborská-oplová,M., Gillet,L., Börner,R., Nues,R.Van, Leitner,A., Michel,E., Petkowski,J.J., Granneman,S., Sigel,R.K.O., *et al.* (2021) Puf6 primes 60S pre-ribosome nuclear export at low temperature. *Nat. Commun.*, **12**, 4696.
21. Lau,B., Huang,Z., Kellner,N., Niu,S., Berninghausen,O., Beckmann,R., Hurt,E. and Cheng,J. (2023) Mechanism of 5S RNP recruitment and helicase-surveilled rRNA maturation during pre-60S biogenesis. *EMBO Rep.*, **24**, e56910.
22. Thoms,M., Kressler,D., Mitterer,V., Kater,L., Falquet,L., Beckmann,R. and Hurt,E. (2018) Suppressor mutations in Rpf2-Rrs1 or Rpl5 bypass the Cgr1 function for pre-ribosomal 5S RNP-rotation. *Nat. Commun.*, **9**, 4094.
23. Barrio-Garcia,C., Thoms,M., Flemming,D., Kater,L., Berninghausen,O., Baßler,J., Beckmann,R. and Hurt,E. (2015) Architecture of the Rix1 – Rea1 checkpoint machinery during pre-60S-ribosome remodeling. *Nat. Struct. Mol. Biol.*, **23**, 37–44.
24. Matsuo,Y., Granneman,S., Thoms,M., Manikas,R.-G., Tollervey,D. and Hurt,E. (2014) Coupled GTPase and remodelling ATPase activities form a checkpoint for ribosome export. *Nature*, **505**, 112–116.
25. Ohmayer,U., Gamalinda,M., Sauert,M., Ossowski,J., Pöll,G., Linnemann,J., Hierlmeier,T., Perez-fernandez,J., Kumcuoglu,B., Leger-silvestre,I., *et al.* (2013) Studies on the assembly characteristics of large subunit ribosomal proteins in *S. cerevisae*. *PLoS One*, **8**, 1–24.
26. Longtine,M.S., McKenzie,A., Demarini,D.J., Shah,N.G., Wach,A., Brachat,A., Philippsen,P. and Pringle,J.R. (1998) Additional modules for versatile and economical PCR-based gene deletion and modification in *Saccharomyces cerevisiae*. *Yeast*, **14**, 953–961.
27. Gietz,D., St,A., Robin,J. and Schiestl,R.H. (1992) Improved method for high efficiency transformation of intact yeast cells. *Nucleic Acids Res.*, **20**, 1992.

28. Janke,C., Magiera,M.M., Rathfelder,N., Taxis,C., Reber,S., Maekawa,H., Moreo-Borchart,A., Doenges,G., Schwob,E., Schiebel,E., *et al.* (2004) A versatile toolbox for PCR-based tagging of yeast genes: new fluorescent proteins, more markers and promoter substitution cassettes. *Yeast*, **21**, 947–962.
29. Thoms,M., Thomson,E. and Hurt,E. (2015) The exosome is recruited to RNA substrates through specific adaptor proteins. *Cell*, **162**, 1029–1038.
30. Jones,G.M., Stalker,J., Humphray,S., West,A., Cox,T., Rogers,J., Dunham,I. and Prelich,G. (2008) A systematic library for comprehensive overexpression screens in *Saccharomyces cerevisiae*. *Nat. Methods*, **5**, 239–241.
31. Sikorski,R. and Heiter,P. (1989) A system of shuttle vectors and yeast host strains designed for efficient manipulation of DNA in *Saccharomyces ceravisiae*. *Genetics*, **122**, 19–27.
32. Horsey,E.W., Jakovljevic,J., Miles,T.D., Harnpicharnchai,P. and Woolford,J.L. (2004) Role of the yeast Rrp1 protein in the dynamics of pre-ribosome maturation. *RNA*, **10**, 813–827.
33. Ulbrich,C., Diepholz,M., Baßler,J., Kressler,D., Pertschy,B., Galani,K. and Bo,B. (2009) Mechanochemical removal of ribosome biogenesis factors from nascent 60S ribosomal subunits. *Cell*, **138**, 911–922.
34. Gadal,O., Strauß,D., Kessl,J., Trumpower,B., Tollervey,D. and Hurt,E. (2001) Nuclear export of 60S ribosomal subunits depends on Xpo1p and requires a nuclear export sequence-containing factor, Nmd3p, that associates with the large subunit protein Rpl10p. *Mol. Cell. Biol.*, **21**, 3405–3415.
35. Wilson,D.M., Li,Y. and Woolford,J.L. (2020) Structural insights into assembly of the ribosomal nascent polypeptide exit tunnel. *Nat. Commun.*, **11**, 1–15.
36. Harnpicharnchai,P., Jakovljevic,J., Horsey,E., Miles,T., Roman,J., Rout,M., Meagher,D., Imai,B., Guo,Y., Brame,C.J., *et al.* (2001) Composition and functional characterization of yeast 66S ribosome assembly intermediates. *Mol. Cell*, **8**, 505–515.
37. Chen,W., Xie,Z., Yang,F. and Ye,K. (2017) Stepwise assembly of the earliest precursors of large ribosomal subunits in yeast. *Nucleic Acids Res.*, **45**, 6837–6847.
38. Micic,J., Li,Y., Wu,S., Wilson,D., Tutuncuoglu,B., Gao,N. and Woolford,J.L. (2020) Coupling of 5S RNP rotation with maturation of functional centers during large ribosomal subunit assembly. *Nat. Commun.*, **11**, 5111.
39. Fromm,L., Falk,S., Flemming,D., Schuller,J.M., Thoms,M., Conti,E. and Hurt,E. (2017) Reconstitution of the complete pathway of ITS2 processing at the pre-ribosome. *Nat. Commun.*, **8**, 1–11.
40. Gasse,L., Flemming,D. and Hurt,E. (2015) Coordinated ribosomal ITS2 RNA processing by the las1 complex integrating endonuclease, polynucleotide kinase, and exonuclease activities. *Mol. Cell*, **60**, 808–815.
41. Biedka,S., Micic,J., Wilson,D., Brown,H., Toth,L.D. and Jr,J.L.W. (2018) Hierarchical recruitment of ribosomal proteins and assembly factors remodels nucleolar pre-60S ribosomes. *J. Cell Biol.*, **217**, 2503–2518.
42. Sarkar,A., Thoms,M., Barrio-Garcia,C., Thomson,E., Flemming,D., Beckmann,R. and Hurt,E. (2017) Preribosomes escaping from the nucleus are caught during translation by cytoplasmic quality control. *Nat. Struct. Mol. Biol.*, **24**, 1107–1115.
43. Kressler,D., Roser,D., Pertschy,B. and Hurt,E. (2008) The AAA ATPase Rix7 powers progression of ribosome biogenesis by stripping Nsa1 from pre-60S particles. *J. Cell Biol.*, **181**, 935–944.
44. Kofler,L., Prattes,M. and Bergler,H. (2020) From snapshots to flipbook — resolving the dynamics of ribosome biogenesis with chemical probes. *Int. J. Mol. Sci.*, **21**, 2998.
45. Pertschy,B., Saveanu,C., Zisser,G., Lebreton,A., Tengg,M., Jacquier,A., Liebminger,E., Nobis,B., Kappel,L. and Klei,I.VanDer (2007) Cytoplasmic recycling of 60S preribosomal factors depends on the AAA protein Drg1. *Mol. Cell. Biol.*, **27**, 6581–6592.
46. Sahasranaman,A., Dembowski,J., Strahler,J., Andrews,P. and Jr,J.L.W. (2011) Assembly of Saccharomyces cerevisiae 60S ribosomal subunits: role of factors required for 27S pre-rRNA processing. *EMBO J.*, **30**, 4020–4032.
47. Wang,Y. and DiMario,P. (2017) Loss of Drosophila nucleostemin 2 (NS2) blocks nucleolar release of the 60S subunit leading to ribosome stress. *Chromosoma*, **126**, 375–388.
48. Ramos-Sáenz,A., González-Álvarez,D., Rodríguez-Galán,O., Rodríguez-Gil,A., Gaspar,S.G., Villalobo,E., Dosil,M. and De La Cruz,J. (2019) Pol5 is an essential ribosome biogenesis factor required for 60S ribosomal subunit maturation in *Saccharomyces cerevisiae*. *RNA*, **25**, 1561–1575.
49. Zhang,H., Elbaum-Garfinkle,S., Langdon,E.M., Taylor,N., Occhipinti,P., Bridges,A.A., Brangwynne,C.P. and Gladfelter,A.S. (2015) RNA controls PolyQ protein phase transitions. *Mol. Cell*, **60**, 220–230.
50. Jain,A. and Vale,R.D. (2017) RNA phase transitions in repeat expansion disorders. *Nature*, **546**, 243–247.
51. Berry,J., Weber,S.C., Vaidya,N., Haataja,M., Brangwynne,C.P. and Weitz,D.A. (2015) RNA transcription modulates phase transition-driven nuclear body assembly. *Proc. Natl. Acad. Sci. U.S.A.*, **112**, E5237–E5245.
52. Uversky,V.N. (2019) Intrinsically disordered proteins and their 'Mysterious' (meta)physics. *Front. Phys.*, **7**, 8–23.
53. Yang,P., Mathieu,C., Kolaitis,R.M., Zhang,P., Messing,J., Yurtsever,U., Yang,Z., Wu,J., Li,Y., Pan,Q., *et al.* (2020) G3BP1 is a tunable switch that triggers phase separation to assemble stress granules. *Cell*, **181**, 325–345.
54. Protter,D.S.W., Rao,B.S., Van Treeck,B., Lin,Y., Mizoue,L., Rosen,M.K. and Parker,R. (2018) Intrinsically disordered regions can contribute promiscuous interactions to RNP granule assembly. *Cell Rep.*, **22**, 1401–1412.
55. Mittag,T. and Parker,R. (2018) Multiple modes of protein–protein interactions promote RNP granule assembly. *J. Mol. Biol.*, **430**, 4636–4649.
56. Carol,S.D. and Noller,H.F. (1993) A cold-sensitive mutation in 16S rRNA provides evidence for helical switching in ribosome assembly. *Genes Dev.*, **7**, 660–670.
57. Dammel,C.S. and Noller,H.F. (1995) Suppression of a cold-sensitive mutation in 16S rRNA by overexpression of a novel ribosome-binding factor, RbfA. *Genes Dev.*, **9**, 626–637.
58. Vanden Broeck,A. and Klinge,S. (2023) Principles of human pre-60S biogenesis. *Science*, **381**, eadh3892.

Received: April 15, 2022. **Revised:** September 11, 2023. **Editorial Decision:** September 18, 2023. **Accepted:** September 22, 2023